A novel control architecture for floating wind turbines

Hegazy, A.; Naaijen, P.; van Wingerden, J. W.

DOI
10.1016/j.ifacol.2023.10.1163

Publication date
2023

Document Version
Final published version

Published in
IFAC-PapersOnLine

Available online at www.sciencedirect.com

ScienceDirect

IFAC PapersOnline CONFERENCE PAPER ARCHIVE

IFAC PapersOnLine 56-2 (2023) 7644–7649

A novel control architecture for floating wind turbines

A. Hegazy * **P. Naaijen** ** **J.W. van Wingerden** *

* *Delft Center for Systems and Control, Delft University of Technology, Delft, 2628 CD, The Netherlands (e-mail: {a.r.hegazy, j.w.vanwingerden}@tudelft.nl)*

** *Maritime and Transport Technology, Delft University of Technology, Delft, 2628 CD, The Netherlands (e-mail: p.naaijen@tudelft.nl)*

Abstract: The control of Floating Wind Turbines (FWTs) is challenging, as they possess much lower natural frequencies related to the structure's rigid body motion, which creates an undesirable coupling between tower motion and the blade pitch control. As a result, the tower motion is negatively damped triggering instability. This is because of the presence of Right Half Plane Zeros (RHPZs) imposing fundamental limitation on the control bandwidth. To address this problem, different solutions were proposed with varying control structures ranging from Single-Input, Single-Output (SISO) controllers to Multiple-input, Multiple-output (MIMO) ones. In this paper, a new control structure, of Single-Input, Multiple-Output (SIMO) is proposed that is able to lift the bandwidth limitation, while using simple elements that match the industry demands.

Keywords: Floating wind turbines, negative damping, multivariable control, $\mathcal{H}_\infty$ control, fixed-structure control.

1. INTRODUCTION

During model experiments of Floating Wind Turbines (FWTs), Nielsen et al. (2006) observed that the conventional blade pitch control, for above rated wind speeds, excites the platform pitch mode, causing unacceptable tower motions. Larsen and Hanson (2007) explained that the blade pitch controller used to regulate the rotor speed, modifies both the aerodynamic torque and thrust, which directly contributes as aerodynamic damping coupling the rotor with the platform pitch dynamics. This coupling is not unique for FWTs though, as Leithead and Dominguez (2006) showed that it also existed in onshore turbines, due to tower fore-aft bending mode. The aerodynamic damping varies with the wind speed, as it is positive in the below-rated region, but negative in the above-rated one, Larsen and Hanson (2007); Jonkman (2008); van der Veen et al. (2012). The main difference is that the fore-aft frequency is significantly lower for FWTs. Usually, the baseline control bandwidth is below the eigenfrequency of the first tower fore-aft mode for onshore turbines, which exceeds the platform pitch eigenfrequency for FWTs. Therefore, the controller may cause severe instability amplifying the tower motion, Larsen and Hanson (2007); Jonkman (2008), as illustrated in Fig. 1.

Larsen and Hanson (2007), and Jonkman (2008) proposed reducing the control bandwidth below the floating platform pitch eigenfrequency while keeping the Single-input, Single-output (SISO) blade pitch Proportional-Integral (PI) control structure. However, this makes the controller react very slowly to the rotor speed oscillations, Fischer (2013). Jonkman (2008), and van der Veen et al. (2012) implemented an extra loop to add damping by feeding back the tower-top motion to the blade pitch via a proportional (P) controller. This requires an extra sensor, hence, called Multiple-Input, Single-Output (MISO) controller, which slightly improve the performance, yet with limited bandwidth, as the RHPZs persist. Multiple-Input, Multiple-Output (MIMO) controllers can help increase the controller bandwidth beyond the platform pitch eigenfrequency, and thus, overcome the bandwidth limitation, Lemmer et al. (2020). Accordingly, Fischer (2013) proposed a MIMO controller by using the generator torque as an extra actuator instead of the blade pitch in the MISO case, as the tower-top velocity is fed back to the generator torque this time using a decentralized MIMO controller. As a result, the bandwidth limitation vanishes, as the extra loop compensates for the Right Half Plane Zeros (RHPZs). Later, Fischer and Loepelmann (2016) reported that feeding back the platform pitch velocity instead is preferable, as it provides extra filtering. Moreover, centralized model-based control approaches as $\mathcal{H}_\infty$, Linear Quadratic Regulator (LQR), and Non-inear Model Predictive Control (NMPC) discussed in the liturature, Lemmer et al. (2020). Furthermore, feedforward control has proven to be a promising technology with the help of wind and wave previews, Navalkar et al. (2015); Al et al. (2020).

The contribution of this paper is twofold:

(1) We show that a Single-Input, Multiple-Output (SIMO) feedback controller, relying on the rotor speed measurement as a single input, and both the blade pitch and generator torque as multiple outputs, also lifts the RHPZs limitation.

10.1016/j.ifacol.2023.10.1163

(2) A fixed-structure feedback controller, based on the synthesized SIMO controller, is introduced to meet the industrial demand for low-order parameterized controllers.

The paper is organized as follows. In Section 2, the FWT model is introduced as well as the negative damping instability. Section 3 demonstrates the different conventional control strategies proposed to tackle that instability. The newly developed control structure is explained in Section 4. Finally, the results of the optimized controller are discussed in Section 5 before concluding in Section 6.

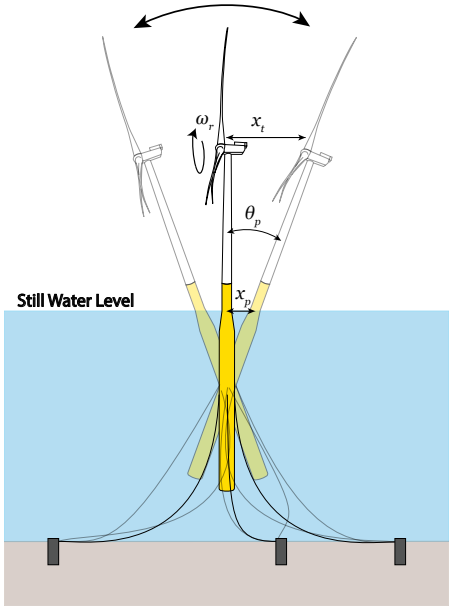

Fig. 1. A scenario where the platform pitch, θ_p, creates a platform surge, x_p, at the center of flotation. Similarly, this pure platform pitching creates a linear tower top displacement, x_t, at the nacelle.

2. FLOATING WIND TURBINE DESCRIPTION

For this study, we used the NREL 5 MW Reference Wind Turbine (RWT), Jonkman et al. (2009), atop the OC3 spar floating platform, Jonkman (2010).

It is worth mentionioning that the controllers in this paper are investigated at wind speed 14 m/s.

2.1 Floating Wind Turbine Model

To address the problem, a simplified mathematical model including the rigid body platform pitch mode in still water, and the rotor dynamics, is used. Equation (1) describes the FWT dynamics in the pitch mode as:

$$M_t\ddot{\theta}_p + B_t\dot{\theta}_p + K_t\theta_p = F_{th}l_{hub}, \tag{1}$$

where θ_p is the platform-pitch angle (rad), $\dot{\theta}_p$ is the platform-pitch velocity (rad/s), $\ddot{\theta}_p$ is the platform-pitch acceleration (rad/s^2), M_t is the overall mass comprising both the structural and added masses of the FWT in pitch, B_t is the overall damping including the hydrodynamic radiation damping and the linearized viscous damping in pitch, K_t is the overall stiffness including the hydrodynamic stiffness and the linearized mooring stiffness in pitch, F_{th} is the thrust force (N), and l_{hub} is the hub height (m). With the thrust force expressed in equation (2).

$$\begin{aligned} F_{th} &= \frac{1}{2}\rho\pi R^2 v_{rel}^2 C_T(\lambda,\beta_c) \\ &= \frac{1}{2}\rho\pi R^2 (v - l_{hub}\dot{\theta}_p)^2 C_T\left(\frac{\omega_r R}{v_{rel}},\beta_c\right), \end{aligned} \tag{2}$$

where ρ is the air density (kg/m^3), R is the rotor diameter (m), v_{rel} is the rotor effective wind speed (m/s), v is the free-stream wind speed (m/s), C_T is the thrust coefficient, λ is the tip speed ratio, ω_r is the rotor speed (rad/s), and β_c is the blade pitch angle (rad).

The surge mode is acceptably damped by the mooring lines, thus not considered, Lemmer et al. (2020). Unlike the surge mode, the pitch mode is insufficiently damped, hence, motions increase uncontrollably in this mode. Only F_{th} is considered because of the coupling between the blade pitch control and the aerodynamic thrust. However, there is no coupling between the wave forces and the pitch control, and thus, waves are excluded.

To explicitly see the effect of F_{th} on the platform-pitch damping, F_{th} is linearized around an operating point, and θ_p, is replaced with the tower-top translational displacement, x_t. As for small pitch angles, $x_t = l_{hub}\theta_p$, this results in equation(3).

$$\begin{aligned} \underbrace{\frac{M_t}{l_{hub}^2}}_{M}\ddot{x}_t + \left(\underbrace{\frac{B_t}{l_{hub}^2}}_{B} + \frac{\partial F_{th}}{\partial v}\right)\dot{x}_t + \underbrace{\left(\frac{K_t}{l_{hub}^2}\right)}_{K} x_t = \frac{\partial F_{th}}{\partial \omega_r}\omega_r \\ + \frac{\partial F_{th}}{\partial v}v + \frac{\partial F_{th}}{\partial \beta_c}\beta_c \end{aligned} \tag{3}$$

The rotor is modelled using equation (4) with the aerodynamic torque, τ_g, linearized about an operating point that is a function of the wind speed as:

$$\dot{\omega}_r = \frac{1}{J_d}\left(\frac{\partial \tau_a}{\partial \omega_r}\omega_r - \frac{\partial \tau_a}{\partial v}\dot{x}_t + \frac{\partial \tau_a}{\partial v}v + \frac{\partial \tau_a}{\partial \beta_c}\beta_c - N_g\tau_g\right) \tag{4}$$

Combining the linear models of the rotor dynamics and the platform pitch described in equation (3) and equation (4), respectively, yields a state space-model with a state vector, $x(t) = [x_t, \dot{x}_t, \omega_r]^{\mathrm{T}}$, and an input vector, $u(t) = [\tau_g, \beta_c, v]^{\mathrm{T}}$. The state-space model following $\dot{x}(t) = Ax(t) + Bu(t)$ is:

$$\dot{x}(t) = \begin{bmatrix} 0 & 1 & 0 \\ -\frac{K}{M} & -\frac{1}{M}\left(B + \frac{\partial F_{Th}}{\partial v}\right) & \frac{1}{M}\frac{\partial F_{Th}}{\partial \omega_r} \\ 0 & -\frac{1}{J_d}\frac{\partial \tau_a}{\partial v} & \frac{1}{J_d}\frac{\partial \tau_a}{\partial \omega_r} \end{bmatrix} \begin{bmatrix} x_t \\ \dot{x}_t \\ \omega_r \end{bmatrix} + \begin{bmatrix} 0 & 0 & 0 \\ 0 & \frac{1}{M}\frac{\partial F_{Th}}{\partial \beta_c} & \frac{1}{M}\frac{\partial F_{Th}}{\partial v} \\ -\frac{N_{gb}}{J_d} & \frac{1}{J_d}\frac{\partial \tau_a}{\partial \beta_c} & \frac{1}{J_d}\frac{\partial \tau_a}{\partial v} \end{bmatrix} \begin{bmatrix} \tau_g \\ \beta_c \\ v \end{bmatrix}, \tag{5}$$

where $\dot{x}(t)$ is the the state derivative vector, A is the system dynamics matrix, and B is the input matrix. The transfer functions in the Laplace domain, $G(s)$, from the inputs, $u(t)$, to the outputs, $y(t) = Cx(t)$, required for the controller design, can be obtained by applying $G(s) = C(sI - A)^{-1}B$. Accordingly, the TF $G_{\beta_c \to \omega_r}$, mapping β_c to ω_r, is:

$$G_{\beta_c \to \omega_r} = \frac{Ms^2 + \left[B + \frac{\partial F_{Th}}{\partial v} - \frac{\partial \tau_a}{\partial v}\frac{\partial F_{Th}}{\partial \beta_c}\left(\frac{\partial \tau_a}{\partial \beta_c}\right)^{-1}\right]s + K}{\left(J_d s - \frac{\partial \tau_a}{\partial \omega_r}\right)\left(Ms^2 + \left[B + \frac{\partial F_{Th}}{\partial v}\right]s + K\right) + \frac{\partial \tau_a}{\partial v}\frac{\partial F_{Th}}{\partial \omega_r}s} \tag{6}$$

Setting the numerator in equation (6) to zero shows that RHPZs emerge if:

$$B < \frac{\partial F_{Th}}{\partial v} - \frac{\partial \tau_a}{\partial v}\frac{\partial F_{Th}}{\partial \beta_c}\left(\frac{\partial \tau_a}{\partial \beta_c}\right)^{-1} \tag{7}$$

Analytically, a complex pair of RHPZs appears in $G_{\beta_c \to \omega_r}$ as shown in equation (7), if the fore-aft dynamics are not sufficiently damped, Fischer (2013). The frequency of the RHPZs always coincides with the fore-aft natural frequencies, like the tower bending modes, and the platform pitch mode. Should the zeros have a positive real part, an inverse-response behavior occurs, posing a hard constraint for control design, Lemmer et al. (2016). Thus, the system becomes unstable if excited at or above the RHPZs frequencies, Larsen and Hanson (2007); Jonkman (2008). The RHPZs are witnessed around the rated wind speed, but disappear from the plant at higher wind speeds as demonstrated in Fig. 2, as they move to the Left Half Plane (LHP) with blade pitching, indicating an increase in the fore-aft damping, Leithead and Dominguez (2006).

3. CONVENTIONAL CONTROL DESIGN

Neglecting the floating platform dynamics during the FWT control design often yields instability in the operating points containing RHPZs. This is because of the high control bandwidth triggered by the high feedback control gains causing platform pitch resonance, Jonkman (2008). At first, one might expect exponential growth in the response due to resonance, but this is not the case due to the non-linear dynamic coupling between the different FWT modes. Yet the FWT keeps oscillating back and forth without reaching steady state, which is still undesirable. There are several ways to mitigate this challenging problem, and thus, in the remainder of this section, the conventional solutions are presented, then followed by our proposed solution in the next section.

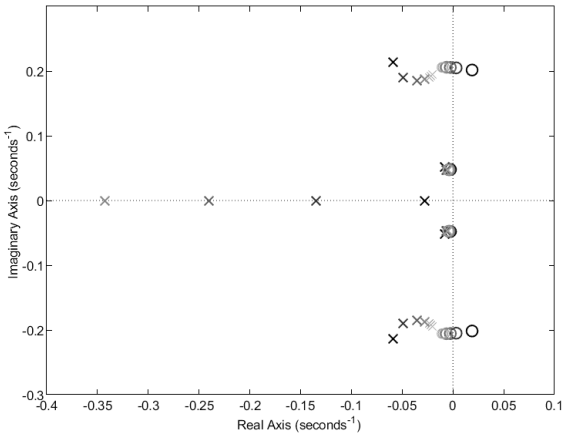

Fig. 2. Pole-zero plot of the TF from blade pitch to rotor speed,$G_{\beta_c \to \omega_r}$, at different wind speeds ranging from 12 m/s (darkest) to 24 m/s (lightest).

3.1 Detuning

One way to overcome resonance is to reduce the bandwidth of the blade pitch controller to be lower than the platform natural frequency, Larsen and Hanson (2007); Jonkman (2008); van der Veen et al. (2012). This leads to overcome resonance, but at the expense of the generator speed tracking performance at the operating points where detuning is applied. A more robust approach uses the linear model to account for the stability margin to be above some threshold, and tunes the controller to the fastest possible response at each operating point, Lemmer et al. (2020).

3.2 Parallel Compensation (MISO & MIMO)

The conventional approach to tackle the negative damping instability includes the closure of a parallel loop, feeding back the tower fore-aft motion, measured at the nacelle. This method is known as "parallel compensation", van der Veen et al. (2012). Parallel compensation can be attained by blade pitch, van der Veen et al. (2012), or generator torque actuators, Fischer (2013), which is a step towards MIMO control. This method attempts to reduce the coupling between the competing aerodynamics of rotor torque and thrust while regulating generator speed through blade pitch. In this study, the fore-aft velocity signal used for parallel compensation is the tower-top pitch rate, which is identical to platform pitch rate assuming a rigid tower. Both blade pitch and generator torque are considered for parallel compensation in this work, and a combination of both is shown to be a good compromise between the benefits and drawbacks of each. In equation (5), element $A(3,2)$ demonstrates the state transition term from the fore-aft motion, $\dot{x}_t$, to the rotor acceleration, $\dot{\omega}_r$. Setting this term to 0 reduces the platform pitching effect on rotor speed tracking. With this tuning method, the parallel compensation feedback does not reduce the platform motion directly, but compensates for the effect that the platform motion has on generator speed regulation instead, which increases the overall closed-loop system stability.

(1) ***Blade pitch*** **(MISO control)**: Parallel compensation using blade pitch feedback, as shown in Fig. 3, is achieved by adding an extra term to element $A(3,2)$, corresponding to the closure of the parallel

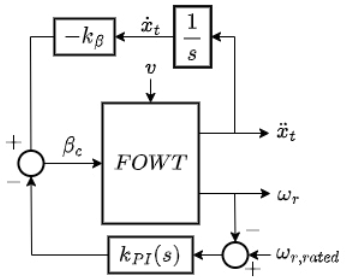

Fig. 3. Block diagram of the blade pitch parallel compensation (MISO controller)

extra feedback loop, where the parallel compensation gain is scheduled to be consistent with the PI controller gains for each operating point. The blade pitch parallel compensation uses proportional feedback of the tower-top velocity due to the platform pitch rate:

$$\beta = -k_\beta \dot{x}_t \tag{8}$$

This extra blade pitch in equation (8) is added to the blade pitch command from the PI controller before the actuator saturation limits are applied. By closing the parallel loop in Fig. 3, a term $k_\beta \frac{1}{J_d} \frac{\partial \tau_a}{\partial \beta_c}$ is subtracted from $A(3,2)$ in equation (5). Solving for a gain that makes $A(3,2) = 0$ leads to full compensation of the effect of platform pitch on the rotor speed. However, due to blade pitch coupling with both aerodynamic torque and thrust, such a gain reduces the effective system fore-aft damping as a side effect. It is, therefore, sensible to choose a smaller gain to partially compensate the fore-aft motion, which can be achieved by multiplying the parallel compensation gain by a static gain, ξ_β,. The parallel compensation gain for blade pitch then becomes

$$K_\beta = -\xi_\beta \frac{\partial \tau_a}{\partial v} \left(\frac{\partial \tau_a}{\partial \beta} \right)^{-1} \tag{9}$$

The sign of ξ_β determines the control objective of the extra blade pitch loop. If $\xi_\beta \in [0,1]$, the effect of the tower-top motion on the rotor speed is thus eliminated at the expense of less fore-aft damping, however, this loop requires extra filtering to change its dynamics, otherwise, it becomes unstable, Abbas et al. (2022). Whereas, if $\xi_\beta \in [-1,0]$, the fore-aft damping is improved, while the drivetrain damping decreases, thus less rotor speed tracking performance. Although the MIMO plant does not have any transmission zeros, the poor rotor speed tracking performance can be referred to the persistence of the RHPZs in $G_{\beta_c \to \omega_r}$, as they are not affected by the parallel loop, and still impose a limitation on the PI controller bandwidth.

(2) ***Generator torque*** **(MIMO control)**: Instead of using the blade pitch in the parallel loop, generator torque can be used instead as illustrated in Fig. 4, and thus taking a step towards MIMO control. Unlike the blade pitch, the generator torque compensation is different as when $G_{\beta_c \to \omega_r}$, is closed with the generator torque parallel loop, the RHPZs move to the LHP. With enough gain, the system becomes minimum phase. At optimal gain, pole-zero cancellation occurs leading the RHPZs to vanish from $\tilde{G}_{\beta_c \to \omega_r}$, which is the TF representing $G_{\beta_c \to \omega_r}$ after closing the generator torque parallel loop. Consequently, the bandwidth of the PI controller can be increased above the platform pitch mode. Applying the same tuning procedure as in blade pitch, we end up with:

$$K_{\tau_g} = \xi_{\tau_g} \frac{1}{N_g} \frac{\partial \tau_a}{\partial v} \tag{10}$$

The main drawback of this approach is the generator torque limit for parallel compensation that can be supplied by the actuator. The usage of the full-compensation gain ($\xi_{\tau_g} = 1$) eliminates the RHPZs, thus, turning the system to minimum phase for all operating points, however, the constraint imposed by the τ_g saturation restrains actuator signals exceeding the maximum generator torque. Reducing the compensation gain with $\xi_{\tau_g} \in [0,1]$ is rather advantageous in practice, as on one hand, it prohibits the generator torque actuator from saturating, and on the other hand, it reduces the drivetrain loads, Fischer (2013). With $\xi_{\tau_g} < 1$, RHPZs are partially compensated giving the opportunity for higher achievable bandwidth, hence, improved performance.

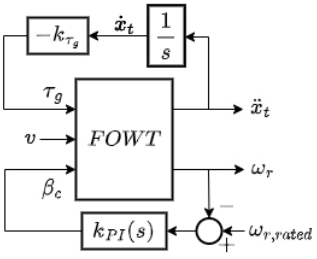

Fig. 4. Block diagram of the generator torque parallel compensation (MIMO controller)

4. SIMO CONTROL

In this section, we present a new control structure, which is illustrated in Fig. 5. In this control structure, we have a SIMO controller that only has the rotor speed error as input, and both the blade pitch and generator torque as outputs. Unlike, the conventional solutions, finding a SIMO controller is not straight forward. So we rely on the $\mathcal{H}_\infty$ formulation for the control synthesis. Based on the synthesized SIMO controller, a fixed structure controller with a matching performance, composed of simple elements, is designed in an industry-standard way.

$\mathcal{H}_\infty$ control synthesis makes use of the general control configuration, in Fig. 6, where P is the generalized plant, and K the synthesized controller. The objective is then to minimize the $\mathcal{H}_\infty$ norm of the transfer function from the exogenous inputs, w, to performance outputs, z, Skogestad and Postlethwaite (2007). The control synthesis problem is then to find a controller, K, that minimizes the infinity norm, $||N||_\infty < 1$.

The generalized plant is typically used to synthesize $\mathcal{H}_2$ or $\mathcal{H}_\infty$ controllers. The advantages of $\mathcal{H}_\infty$ controller design is mainly the ability of shaping closed-loop transfer functions

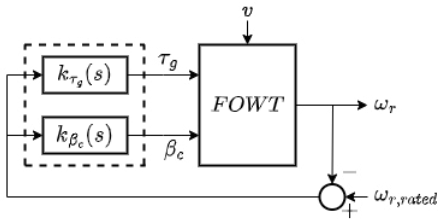

Fig. 5. Block diagram of the SIMO controller enclosed by the dashed lines.

and setting stability and robustness margins. That is in addition to the possibility for extensions to LPV and robust control.

Here, w is considered the reference rotor speed ($w = \omega_{r,ref}$). While two performance signals, z_1 and z_2, are specified, with z_1 represents the weighted response penalized by the weight W_p to reduce the effect of w, and z_2 representing the weighted control action penalized by the weight W_u to bound the actuator limits. Signals v and u represent the control input ($\omega_{r,ref} - \omega_r$) and the control action $[\tau_g, \beta_c]^{\mathrm{T}}$, respectively. As for G, it is TF matrix mapping both τ_g and β_c to ω_r.

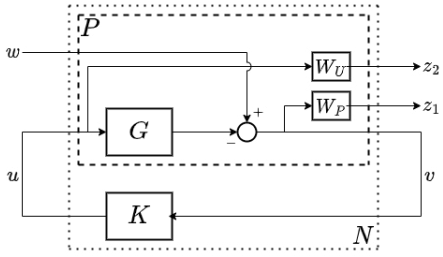

Fig. 6. Block diagram of the generic model of generalized plant and controller. The generalized plant $P(s)$ includes all the elements of the system except the controller $K(s)$.

In this paper, the $\mathcal{H}_\infty$ controller synthesis considers two criteria to design and evaluate the performance of the controller. The sensitivity, S, and the controller sensitivity, KS, which are defined as

$$S = (I + GK)^{-1}, \quad KS = K(I + GK)^{-1}, \tag{11}$$

where S is the TF mapping the disturbance to the system output, while KS is the TF from the disturbance to the control signal. The closed-loop S should be small for low frequencies in order to achieve good disturbance rejection. $W_P(s)$ is chosen to get a slope of 20 dB/dec in $|S|$ for the low frequency region as follows

$$W_P(s) = \frac{s/M + \omega_B}{s + A\omega_B}, \tag{12}$$

where ω_B is the desired closed-loop bandwidth, A is the desired disturbance attenuation within the closed-loop bandwidth, and M is the desired bound on the sensitivity margin, Skogestad and Postlethwaite (2007). The controller sensitivity is penalized at high frequencies by W_U.

As mentioned above, the main benefits of $\mathcal{H}_\infty$ control synthesis is the ability to shape closed-loop frequency responses. The controller is designed such that based on the information in v, a control signal, u, is generated to counteract the influence of the exogenous inputs, w, on the exogenous outputs, z, by minimizing the weighted $\mathcal{H}_\infty$ norm of transfer functions from w to z_1 and z_2. The controller is obtained via the minimization of the mixed-sensitivity problem with respect to the controller K

$$\min_{\mathrm{K}} ||N(K)||_\infty = \left\| \begin{bmatrix} W_P S \\ W_U K S \end{bmatrix} \right\|_\infty \tag{13}$$

Once the $\mathcal{H}_\infty$ SIMO controller is obtained, it serves as a reference for designing a fixed control structure. Subsequently, the fixed-structure could be identified for the SIMO controller, and was found to be composed of an inverted-notch filter at the generator torque input channel, and a PI at the blade pitch input channel as shown in Fig. 5, from which we can observe the significant increase in the bandwidth in both the SIMO $\mathcal{H}_\infty$, and the fixed structure SIMO compared to the rest of the controllers.

5. RESULTS

Following the synthesis of the SIMO $\mathcal{H}_\infty$ controller, it is observed in Fig. 7, that the generator torque channel has a structure close to an inverted notch filter concentrated close to the platform pitch natural frequency, while the blade pitch input channel resembles a simple PI controller. Regarding the RHPZs, we can already see that at the platform pitch eigenfrequency the τ_g channel has a resonance peak to deal with the existing anti-resonance peak in the plant. At the same time, we see in the magnitude plot of the β_c channel that there is no resonant peaks indicating that the PI control is unaffected by the RHPZs anymore.

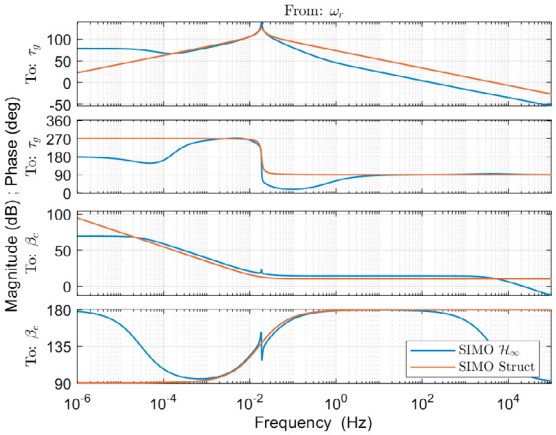

Fig. 7. Comparison between SIMO $\mathcal{H}_\infty$ and the structured SIMO controllers at wind speed 14 m/s.

Although a fixed-structure SIMO controller, that is close to the synthesized SIMO $\mathcal{H}_\infty$ controller, was achieved, however, the fixed-structure controller should be implemented with great caution, as the SIMO $\mathcal{H}_\infty$ one is a feedback controller that does not require any prior loop closures. Whereas, on the other hand, the fixed-structure SIMO control loops can be either simultaneously or sequentially. Assuming sequential loop closure to as a step towards industry, the generator torque loop must be

closed first with the inverted-notch filter to manipulate the RHPZs and move them to another unimportant output channel, before closing the blade pitch loop with the PI controller that, in theory, should have now a much higher bandwidth than the baseline one. In practice, the bandwidth would still be limited by other unstable modes in addition to the actuators' saturation limit as mentioned before. However, the blade pitch loop must not be closed first by any means, otherwise instability occurs.

The performance of the different controllers is compared in a linear fashion using the sensitivity function, S, which is illustrated in Fig. 8.

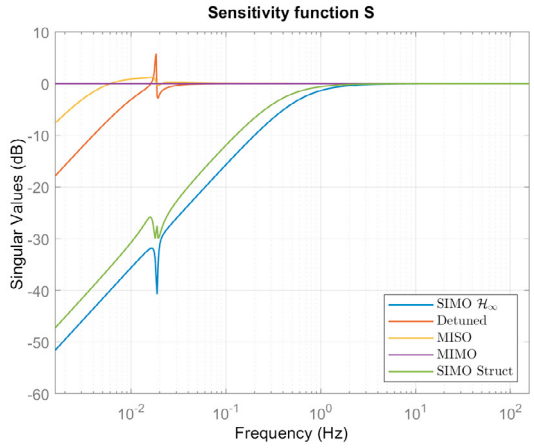

Fig. 8. Sensitivity function of the different controllers at wind speed 14 m/s.

Fig. 8 shows the superiority of the SIMO controller compared to the other ones. As it is clear how high the closed-loop bandwidth can be compared to the other cases, where the bandwidth is defined as the frequency where the sensitivity crosses -3 dB from below. This indicates that the RHPZs bandwidth limitation is lifted with the SIMO controller. It also shows that with just a single measurement (rotor speed), a controller exists that can tackle the negative damping instability, instead of using a second measurement (tower-top motion) and turn into full MIMO control.

6. CONCLUSION

A generalised framework was set up for the $\mathcal{H}_\infty$ synthesis of a SIMO feedback controller for the rotor speed regulation of floating wind turbines, from which, a simple control structure for industry standards, was derived. Rotor speed oscillation minimisation was included in the controller synthesis. An $\mathcal{H}_\infty$ SIMO controller was obtained that was then reduced to a fixed-structure SIMO controller, which is composed of simple elements as an inverted-notch and a PI controller. Though, should sequential loop closure is appliead to the fixed-structure controller, the correct order of loop closures must be followed, otherwise instability arises.

ACKNOWLEDGEMENTS

This project is part of the FLOATECH project. The research presented in this paper has received funding from the European Union's Horizon 2020 research and innovation programme under grant agreement No. 101007142.

REFERENCES

Abbas, N.J., Zalkind, D.S., Pao, L., and Wright, A. (2022). A reference open-source controller for fixed and floating offshore wind turbines. 7(3), 53–73. doi:10.5194/wes-7-53-2022.

Al, M., Fontanella, A., van der Hoek, D., Liu, Y., Belloli, M., and van Wingerden, J.W. (2020). Feedforward control for wave disturbance rejection on floating offshore wind turbines. In *Journal of Physics: Conference Series*, volume 1618, 022048. IOP Publishing.

Fischer, B. (2013). Reducing rotor speed variations of floating wind turbines by compensation of non-minimum phase zeros. 7(4), 413–419. doi:10.1049/iet-rpg.2012.0263.

Fischer, B. and Loepelmann, P. (2016). Balancing rotor speed regulation and drive train loads of floating wind turbines. In *Journal of Physics: Conference Series*, volume 753, 052016. IOP Publishing.

Jonkman, J., Butterfield, S., Musial, W., and Scott, G. (2009). Definition of a 5-MW reference wind turbine for offshore system development. doi:10.2172/947422.

Jonkman, J. (2008). Influence of control on the pitch damping of a floating wind turbine. In *46th AIAA Aerospace Sciences Meeting and Exhibit*. American Institute of Aeronautics and Astronautics. doi:10.2514/6.2008-1306.

Jonkman, J. (2010). Definition of the floating system for phase iv of oc3. Technical report, National Renewable Energy Lab.(NREL), Golden, CO (United States).

Larsen, T.J. and Hanson, T.D. (2007). A method to avoid negative damped low frequent tower vibrations for a floating, pitch controlled wind turbine. 75, 012073. doi:10.1088/1742-6596/75/1/012073.

Leithead, W.E. and Dominguez, S. (2006). Coordinated control design for wind turbine control systems.

Lemmer, F., Schlipf, D., and Cheng, P.W. (2016). Control design methods for floating wind turbines for optimal disturbance rejection. In *Journal of Physics: Conference Series*, volume 753, 092006. IOP Publishing.

Lemmer, F., Yu, W., Schlipf, D., and Cheng, P.W. (2020). Robust gain scheduling baseline controller for floating offshore wind turbines. 23(1), 17–30. doi:10.1002/we.2408.

Navalkar, S.T., van Wingerden, J.W., Fleming, P.A., and Van Kuik, G. (2015). Integrating robust lidar-based feedforward with feedback control to enhance speed regulation of floating wind turbines. In *2015 American Control Conference (ACC)*, 3070–3075. IEEE.

Nielsen, F.G., Hanson, T.D., and Skaare, B. (2006). Integrated dynamic analysis of floating offshore wind turbines. 671–679. ASMEDC. doi:10.1115/OMAE2006-92291.

Skogestad, S. and Postlethwaite, I. (2007). *Multivariable Feedback Control: Analysis and Design*. John Wiley & Sons.

van der Veen, G.J., Couchman, I.J., and Bowyer, R. (2012). Control of floating wind turbines. In *2012 American Control Conference (ACC)*, 3148–3153. IEEE. doi:10.1109/ACC.2012.6315120.